Biomineralization

DOI: 10.1002/anie.201103407

Structure and Mechanical Properties of a Pteropod Shell Consisting of Interlocked Helical Aragonite Nanofibers**

Taiji Zhang, Yurong Ma, Kai Chen, Martin Kunz, Nobumichi Tamura, Ming Qiang, Jun Xu, and Limin Qi**

Most biominerals, such as bones,[1] teeth,[2] nacre,[3] sponges,[4] conch shells,[5] and sea urchin teeth,[6] have exceptional mechanical properties far beyond those that can be achieved using synthetic materials with the same components. This is mainly due to their complex hierarchical heterogeneous microstructures.[7] For example, nacre is mainly composed of aragonite platelets; however, its toughness is 3000 times higher than synthetic aragonite. The unique "bricks and mortar" structure in nacre and the combination of mineral and organic layers contribute to the excellent toughness of nacre.[8] Some arthropod exoskeletons, such as those of crabs and lobsters, possess twisted plywood-type structures, which contribute to their sophisticated anisotropic mechanical properties.[9]

Pteropods are a group of planktonic gastropods that have ultrathin lightweight mineralized shells composed of aragonite.[10] Pteropods are a major planktonic producer of aragonite in seawater. Their shells are affected by the CO_2 concentration in the atmosphere and could act as a biological indicator for changes in the atmospheric CO_2 concentration.[11] In 1972, Bé and co-workers reported a novel helical structure in the shell of the pteropod *Cuvierina columnella* by examining fracture sections using scanning electron microscopy (SEM).[10a] Follow-up work also showed this helical structure in other pteropod species.[12] However, there is no direct evidence for the existence of this novel helical structure, and the function of this special hierarchical structure remains unknown. Herein, for the first time, the hierarchical microstructures and crystallographic orientations of the shells of the pteropod *Cavolinia uncinata* (*CU*) were studied in detail by using a combination of techniques, and further mechanical property tests indicate that the *CU* shell has anisotropic mechanical properties, which is probably due to its helical microstructure and crystal alignment.

The *CU* shell is about five millimeters in length (Figure 1 a). The dorsal part of the pteropod shell has a thickness of about 10–20 μm; that is, significantly thinner than the thickness of the abdominal part of the shell (20–30 μm). Both the IR spectrum and XRD pattern show that the mineral in *CU* shell is aragonite (Supporting Information, Figure S1), a polymorph found in many other biominerals, such as nacre and conch shells.[7a] Figure 1 b–e show that the fracture sections of the abdominal part are composed of densely packed curved nanofibers. Figure 1 c displays the curved

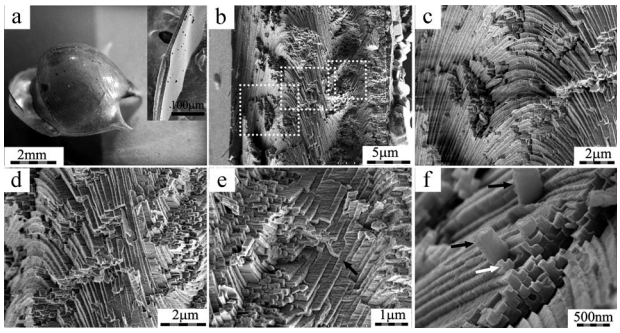

Figure 1. a) Photograph of a whole *CU* shell, including the abdominal (top) and the dorsal parts (bottom). Inset: an SEM image of a vertical abdominal shell fragment, exposing a fracture section. b–f) Enlarged SEM images of the shell fracture section in (a). b) The whole fracture section at low magnification; boxed regions are enlarged in (c–e). c) The left slope of the fracture section, where the fibers are bent and form arc-shaped structures. d) The ridgeline area, where the fibers are parallel to the cross-section. e) The right slope; the arrow indicates the bottom of the right valley. f) The cross-sections of the nanofibers possess an inter-locked mosaic structure. Most fibers have an L- or T-shaped cross-section.

[*] T. Zhang, Prof. Y. Ma, Prof. L. Qi
Beijing National Laboratory for Molecular Sciences, State Key Laboratory for Structural Chemistry of Unstable and Stable Species, College of Chemistry, Peking University (PKU)
Beijing 100871 (China)
E-mail: yurong.ma@pku.edu.cn
liminqi@pku.edu.cn

M. Qiang
College of Engineering, PKU
Beijing 100871 (China)

Dr. J. Xu
School of Physics, PKU
Beijing 100871 (China)

Dr. K. Chen
National Center for Electron Microscopy, Lawrence Berkeley National Laboratory (LBNL)
1 Cyclotron Road, Berkeley, CA 94720 (USA)

Dr. M. Kunz, Dr. N. Tamura
Advanced Light Source, LBNL
Berkeley, CA 94720 (USA)

[**] We thank Steve Weiner and Lia Addadi for fruitful discussions and Pupa Gilbert for kindly sharing her X-ray microdiffraction beamtime. Financial support from the National Basic Research Program of China (Grant Nos. 2007CB815602, 2007CB936201) and NSFC (Grant Nos. 50902002, 20873002, 21073005, and 50821061) is gratefully acknowledged. The Advanced Light Source is supported by the Director, Office of Science, Office of Basic Energy Sciences, Materials Science Division, of the U.S. Department of Energy under Contract No. DE-AC02-05CH11231 at LBNL.

Supporting information for this article is available on the WWW under http://dx.doi.org/10.1002/anie.201103407.

nanofibers with a bending angle larger than 90° on the left slope and Figure 1 d demonstrates how the ridge area of the fracture section is composed of densely packed nanofibers, which are generally flat on the top ridgeline area, but slope down on both sides. Moreover, these curved nanofibers are continuous from the left shell side to the right side. This is in contrast to the twisted plywood-style microstructures composed of straight nanorods found in other biomaterials, such as conch shells[5] and marine arthropod exoskeletons.[9b] The nanofibers have irregular cross-sections, such as T-shaped, L-shaped, rectangular, or other irregular shapes, and they form an interlocked mosaic microstructure (Figure 1 f; Supporting Information, Figure S2), which seems to make the nanofiber difficult to remove from the shell (marked with black arrows in Figure 1 f).

These nanofibers bend clockwise while passing through the shell. They are not wave-like or circular structures, and it is proposed that the nanofibers are right-handed tightly packed helical microstructures with the helical axis perpendicular to the shell surface. The nanofibers go through 1.3 leads of the helix from one side to the other side of the shell. The tightly packed helical microstructure is more obvious in Figure 2 a. The helical diameter and lead are about 20–25 μm and 10–16 μm, respectively, and the helix angle is about 26–34° (Figure 2 b). A 2D model composed of single-layer densely packed helical fibers was built by using the model helical fiber shown in Figure 2 b as the building unit (Figure 2 c). This model perfectly consistent with the real shell fracture section if the cross-sections of the broken nanofibers in Figure 2 a are ignored. The ridge area in the middle and the two slope areas can be seen more clearly if the shell fracture section is tilted to different angles, namely −30, 0, and 30° (Figure 2 d–f). The morphologies of fracture section models after tilting to −30, 0, and 30° (Figure 2 g–i) are fully consistent with the respective SEM images of fracture sections. Furthermore, based on the SEM images of the fracture sections of the inner and outer shell surface (Supporting Information, Figure S3, S4), a multilayer 3D model was also constructed, which was perfectly consistent with the original shell structure from more than one observation direction (Supporting Information, Figure S5). The above SEM images and simulations provide strong evidence that the nanofibers in the *CU* shell are actually right-handed helical microstructures.

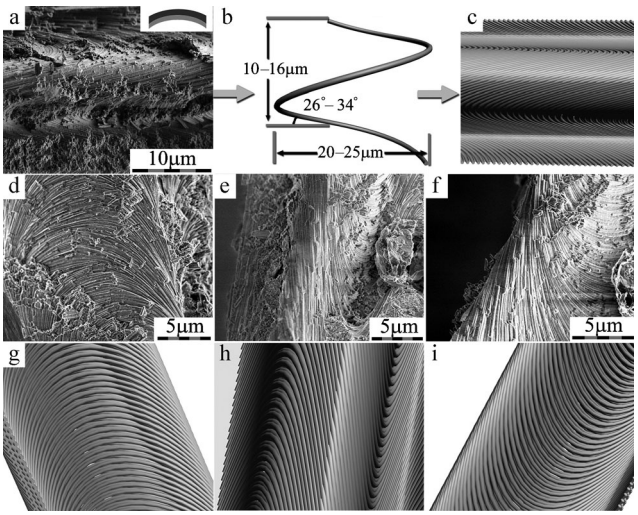

Figure 2. SEM images of fracture sections of *CU* shell and their corresponding 2D models. a) A typical fracture section of *CU* shell. Inset: a model of a shell fragment. b) A right-handed helical fiber that corresponds to the helical structure in (a) as a subunit for the 2D model. c) A 2D model, comprising a single layer of densely packed right-handed helical nanofibers aligned in parallel. d–f) The same fracture section of *CU* shell tilted at different angles: −30, 0, and 30°, respectively. g–i) The single-layer model, also tilted at angles of −30, 0, and 30°, respectively, to simulate the fracture sections in (d–f).

Further evidence of the helical nanofibers in pteropods is given by environmental SEM (ESEM) characterization. Two preformed microholes were used as markers, and the area located at the center of two markers was characterized under ESEM (Supporting Information, Figure S6a). The exposed section was polished in 1 μm steps along the direction perpendicular to the shell surface from the outer surface and characterized by ESEM repeatedly, thus exposing cross-sections from the same area but at different depths, until the inner surface was reached. Some selected ESEM images are shown in the Supporting Information, Figure S6b–h. After each polishing cycle, parts of the continuous helical nanofibers were cut off, and well-aligned oblique cross-sections with broken tips were created. It is noteworthy that these oblique cross-sections of nanofibers that arise from the bottom are clearly different from the twisted plywood-like straight rods existing in arthropod exoskeletons.[9b] The alignment directions turn clockwise after polishing layer by layer. The elongating cross-sections of the nanofibers (Supporting Information, Figure S6i) rotate for almost 300° from (6b) to (6h), and this agrees well with the right-handed helical structure. We also used a shell model to simulate these exposed cross-sections after layer-by-layer polishing (Supporting Information, Figure S7) and the simulation results are consistent with the experimental results. This is another convincing evidence for the helix assembly microstructure in *CU* shell.

Diffraction experiments were carried out on *CU* shell by using synchrotron X-ray microdiffraction. Figure 3 a shows the X-ray fluorescence (XRF) map for the calcium XRF window of a thin-shell transverse cross-section with a thickness of about 100 μm used for X-ray microdiffraction. The area marked with a square box in the XRF and light microscopy images (inset of Figure 3 a) was characterized by X-ray microdiffraction. Eight diffraction patterns with an X-ray beam size of 20 μm × 1 μm (H × V FWHM) were taken in the area (30 μm × 40 μm) marked in Figure 3 a. The eight diffraction patterns are nearly identical. The diffraction rings show very localized diffraction intensities, as expected for a single crystal. The simultaneous observation of all accessible rings at one wavelength, however, demonstrates that in fact it is a highly textured powder diffraction pattern with the individual crystallites being much smaller than the probe beam (ca. 20 μm × 2 μm). From the width of the individual peaks along the azimuthal direction (that is, along the

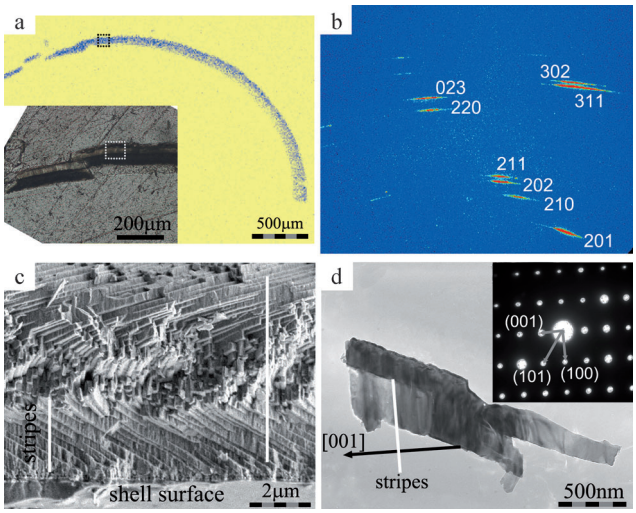

Figure 3. Crystallographic characterization of *CU* shell. a) X-ray fluorescence micrograph of the Ca Kα line and a light microscopy image (inset) of a thin-shell transverse cross-section used for X-ray microdiffraction. b) X-ray microdiffraction pattern from a polished cross-section of the shell. c) SEM image of a shell fracture section showing a series of stripes on the nanofibers, which are all perpendicular to the shell surface. d) TEM image of a nanofiber and the corresponding electron diffraction pattern (inset).

circumference of the diffraction cones), we estimate a misorientation of about 8–10° (Figure 3b). The lattice distances calculated for the diffraction rings are consistent with those of aragonite. Thousands of nanofibers with a diameter about 50–500 nm exist in the thin section with an area of about 1200 μm^2 and probe depth of about 100 μm, providing the crystal powder for the powder patterns. Its intrinsic parallel alignment within the spirals is deemed to be the cause for the highly co-oriented texture of the aragonite nanofibers. The strong co-orientation is also supported by images from polarized light microscopy of a shell fragment (Supporting Information, Figure S8). This co-orientation phenomenon is actually very common in biological minerals and has been observed many times.[7a,13]

Many stripes uniformly distributed on the nanofibers are visible in the SEM images of the fracture sections. (Figure 3c; Supporting Information, Figure S9). Although the nanofibers are helical and thus continuously change their direction, the stripes remain parallel with each other in a direction perpendicular to the shell surface (or parallel to the helix axis). Stripes can also be seen from TEM images (Figure 3d) that are all perpendicular to the [001] direction of aragonite. The selected area electron diffraction pattern (SAED) of one single nanofiber indicates that it is an aragonite single crystal.

Protection is always the most important function for a shell; therefore, we tested the mechanical property of *CU* shell. The shell was polished along two directions, one perpendicular to the shell surface (transverse cross-section, Figure 4a,b,d,e), and one parallel to the shell surface (Figure 4c,f). There are two kinds of microstructures: interlocking mosaic microstructures and needle-like microstructures in the transverse cross-sections. However, only well-aligned cross-sections of the nanofibers appear in the polished section parallel to the shell surface (Figure 4f).

The mechanical properties of *CU* shells were characterized by nanoindentation. Figure 4g shows an AFM image of the polished surface directly after the indentation tests with an indentation depth of 100 nm and with a load of about 1.2–1.3 mN; a 4 × 4 indentation mapping can be clearly seen. The indentations are triangular and about 400 nm in diameter, without any observable cracks at the corners (Figure 4h). The indentation diameter increases with increasing the load force. No cracks can be observed even after indentations under the maximum force of the nanoindenter, namely 10 mN (Supporting Information, Figure S10). The loading force curves in Figure 4i show that a larger force is needed in the shell parallel direction than the normal direction for the same indentation depth, that is, 100 nm. The hardness values of the transverse cross-section and section parallel to the shell surface are almost the same, namely about (5.2 ± 0.4) and (5.6 ± 0.3) GPa, respectively. However, the modulus of the transverse cross-section is (85.9 ± 2.7) GPa, which is significantly higher than that of the section parallel to the surface,

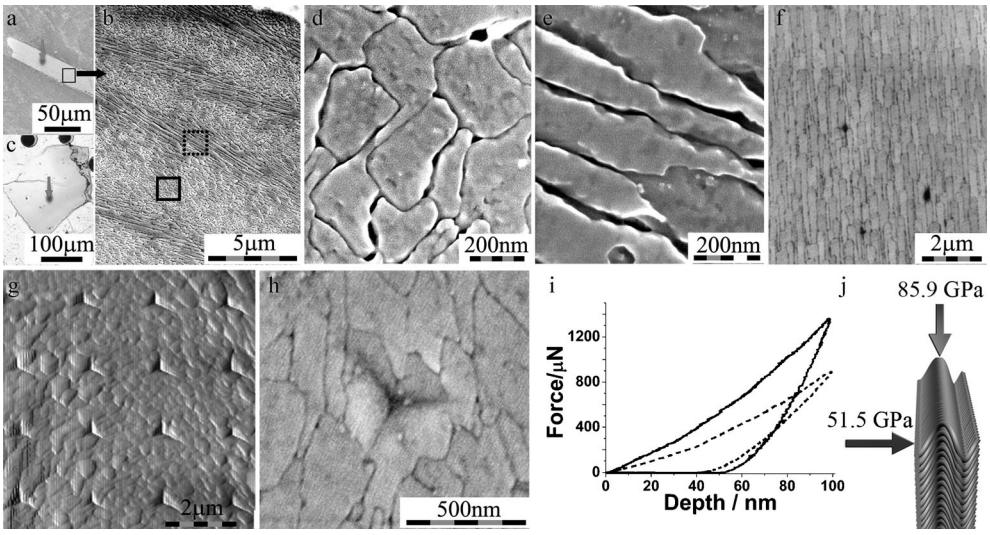

Figure 4. Mechanical characterization of *CU* shell by using nanoindentation. a,b,d,e) SEM images of polished transverse cross-sections perpendicular to the shell surface before nanoindentation. c,f) SEM images of polished sections parallel to the shell surface before nanoindentation. g,h) AFM (g) and SEM (h) images of the polished cross-section after nanoindentation. i) Loading force curves, with the depth obtained from nanoindentation tests on different cross-sections. —— parallel, ----- normal to the shell. j) Diagram of the modulus values along different directions of the shell helix structure.

which is (51.5 ± 1.6) GPa (Figure 4j). The anisotropic mechanical properties in the *CU* shell difference might be due to the densely packed helical nanofiber structure. Similar anisotropic mechanical properties that are due to hierarchical microstructures have been reported in many other biominerals,[7a] such as bone,[1a] tooth,[2] nacre,[3b] lobster exoskeleton,[9b] and wood.[14] It is worthy to note that the Young's modulus and hardness of nacre are about 60–84 GPa and 2.7–6.5 GPa,[15] respectively. Thus the pteropod *CU* shell has hardness and modulus as good as nacre, which is also composed of aragonite and a small amount of organic matrix.

The interlocked mosaic microstructure of the densely packed nanofibers in the *CU* shells is very similar to topological interlocking structure of brick used for construction. Dyskin et al.[16] reported a structure based on matching of contacting surfaces, which exhibits interlocking properties and stays flexible. Such a design renders materials with a high tolerance with respect to local failures, and can be applied to surface protection with brittle material.[16,17] Fratzl et al.[18] also found such an interlocking structure in the suture of turtle shell. The interlocking mosaic structure in *CU* shells probably plays a similar role. As aragonite is brittle,[19] the topological mosaic structure can increase the shell tolerance to brittle failure and makes the shell tougher, as if the shell was built up of normal nanofibers. We indeed found the nanofibers in bundles when breaking them into pieces, and it was difficult to separate a single nanofiber (Figure 1f; Supporting Information, S2), which demonstrates the interlocking effect of the mosaic structure.

Crystallographic co-orientation is another important feature for many biominerals,[1a,6,7a] and is assumed to contribute to the higher mechanical properties in these biominerals.[6] Although arranged in a more complicated way than the other crystallographically oriented biominerals composed of 1D or 2D subunits, in the *CU* shells, the 3D densely packed helical nanofibers show crystallographic alignment with a mutual misorientation of about 10°. This crystallographic co-orientation in *CU* shell might be another important feature contributing to the mechanical properties of this ultrathin lightweight armor of pteropods.

Because *CU* lives at shallow depths in the seawater column, it must keep its shell lightweight. Therefore, their shell formation strategy is different from other mollusks, which possess large and thick shells and live at the bottom of the sea. This special densely packed helical nanofiber structure allows it to decrease the shell thickness to as little as 20 μm, therefore reducing its weight while maintaining sufficient structural strength to protect its soft body. Coiled carbon nanotubes add a nonlinear spring response to their exceptional elastic stiffness and resilience that makes them suitable for protection of devices from impact.[20] We hypothesize that the helix microstructure in *CU* shell also contributes to its anisotropic mechanical properties. Lower modulus in the normal direction of the shell surface means that the shell is flexible on its normal direction, which allows the release of pressure from seawater. This is consistent with the speculation that the adult whorl of thin-shelled species, including pteropods, is rather flexible.[10c,12a]

In conclusion, we have shown the existence of this novel helical nanofiber by using two methods: comparing helical nanofiber simulations and SEM images of fracture sections, and shell-sectioning. Other than the helix feature, the nanofibers in the *CU* shell are all interlocked and crystallographically aligned. Nanoindentation revealed that the modulus on the transverse cross-section is much higher than that on the section parallel to the shell surface while their hardness values are similar. Such anisotropic mechanical properties could be attributed to the existence of the spring-like helical nanofibers in the *CU* shell. All the novel characters of the ultrathin shell, such as the helical nanofibers, the interlocking properties, and the crystallographic orientations, may strengthen the ultrathin armor in pteropods, which may inspire people for the synthesis of ultrathin and/or lightweight engineered materials with superior mechanical properties.

Received: May 18, 2011
Published online: September 26, 2011

Keywords: biomineralization · helical nanofibers · interlocked microstructures · mechanical properties · pteropod shells

[1] a) S. Weiner, H. D. Wagner, *Annu. Rev. Mater. Sci.* **1998**, *28*, 271; b) P. Fratzl, H. S. Gupta, E. P. Paschalis, P. Roschger, *J. Mater. Chem.* **2004**, *14*, 2115.
[2] A. Tencate in *Oral Histology: Development, Structure and Function* (Ed.: A. R. Tencate), Mosby, St. Louis, **1994**, p. 45.
[3] a) B. L. Smith, T. E. Schaffer, M. Viani, J. B. Thompson, N. A. Frederick, J. Kindt, A. Belcher, G. D. Stucky, D. E. Morse, P. K. Hansma, *Nature* **1999**, *399*, 761; b) F. Barthelat, C. M. Li, C. Comi, H. D. Espinosa, *J. Mater. Res.* **2006**, *21*, 1977.
[4] J. Aizenberg, J. C. Weaver, M. S. Thanawala, V. C. Sundar, D. E. Morse, P. Fratzl, *Science* **2005**, *309*, 275.
[5] S. Kamat, X. Su, R. Ballarini, A. H. Heuer, *Nature* **2000**, *405*, 1036.
[6] Y. R. Ma, B. Aichmayer, O. Paris, P. Fratzl, A. Meibom, R. A. Metzler, Y. Politi, L. Addadi, P. U. P. A. Gilbert, S. Weiner, *Proc. Natl. Acad. Sci. USA* **2009**, *106*, 6048.
[7] a) M. A. Meyers, P. Y. Chen, A. Y. M. Lin, Y. Seki, *Prog. Mater. Sci.* **2008**, *53*, 1; b) M. Cusack, A. Freer, *Chem. Rev.* **2008**, *108*, 4433.
[8] a) J. D. Currey, *Proc. R. Soc. London Ser. B* **1977**, *196*, 443; b) H. J. Gao, B. H. Ji, I. L. Jager, E. Arzt, P. Fratzl, *Proc. Natl. Acad. Sci. USA* **2003**, *100*, 5597.
[9] a) P. Romano, H. Fabritius, D. Raabe, *Acta Biomater.* **2007**, *3*, 301; b) H. O. Fabritius, C. Sachs, P. R. Triguero, D. Roobe, *Adv. Mater.* **2009**, *21*, 391.
[10] a) A. W. H. Bé, C. MacClintock, D. C. Curry, *Biomineralization Res. Rep.* **1972**, *4*, 47; b) C. M. Lalli, R. W. Gilmer, *Pelagic snails; the biology of holoplanktonic gastropod molluscs*, Stanford University Press, Stanford, CA, **1989**; c) K. Bandel, C. Hemleben, *Mar. Biol.* **1995**, *124*, 225.
[11] J. C. Orr, V. J. Fabry, O. Aumont, L. Bopp, S. C. Doney, R. A. Feely, A. Gnanadesikan, N. Gruber, A. Ishida, F. Joos, R. M. Key, K. Lindsay, E. Maier-Reimer, R. Matear, P. Monfray, A. Mouchet, R. G. Najjar, G. K. Plattner, K. B. Rodgers, C. L. Sabine, J. L. Sarmiento, R. Schlitzer, R. D. Slater, I. J. Totterdell, M. F. Weirig, Y. Yamanaka, A. Yool, *Nature* **2005**, *437*, 681.
[12] a) R. L. Batten, M. P. Dumont, *Bull. Am. Mus. Nat. Hist.* **1976**, *157*, 263; b) D. Curry, J. Rampal, *Malacologia* **1979**, *18*, 23; c) K.

Bandel, *Shell structure of the Gastropoda excluding the Archaeogastropoda*, *Vol. 1*, Van NostrandReinolds, New York, **1990**.
[13] a) J. Aizenberg, A. Tkachenko, S. Weiner, L. Addadi, G. Hendler, *Nature* **2001**, *412*, 819; b) Y. Politi, T. Arad, E. Klein, S. Weiner, L. Addadi, *Science* **2004**, *306*, 1161; c) H. D. Espinosa, J. E. Rim, F. Barthelat, M. J. Buehler, *Prog. Mater. Sci.* **2009**, *54*, 1059.
[14] R. Menig, M. H. Meyers, M. A. Meyers, K. S. Vecchio, *Acta Mater.* **2000**, *48*, 2383.
[15] a) F. D. Fleischli, M. Dietiker, C. Borgia, R. Spolenak, *Acta Biomater.* **2008**, *4*, 1694; b) J. Y. Sun, J. Tong, *J. Bionic Eng.* **2007**, *4*, 11; c) K. Katti, D. R. Katti, J. Tang, S. Pradhan, M. Sarikaya, *J. Mater. Sci.* **2005**, *40*, 1749.
[16] A. V. Dyskin, Y. Estrin, E. Pasternak, H. C. Khor, A. J. Kanel-Belov, *Adv. Eng. Mater.* **2003**, *5*, 116.
[17] A. V. Dyskin, Y. Estrin, A. J. Kanel-Belov, E. Pasternak, *Phys. Lett. A* **2003**, *319*, 373.
[18] S. Krauss, E. Monsonego-Ornan, E. Zelzer, P. Fratzl, R. Shahar, *Adv. Mater.* **2009**, *21*, 407.
[19] A. P. Jackson, J. F. V. Vincent, R. M. Turner, *Proc. R. Soc. London Ser. B* **1988**, *234*, 415.
[20] C. Daraio, V. F. Nesterenko, S. Jin, W. Wang, A. M. Rao, *J. Appl. Phys.* **2006**, *100*, 064309.

